J Mol Model (2010) 16:1159–1168
DOI 10.1007/s00894-009-0629-4

ORIGINAL PAPER

Mechanism of CDK5 activation revealed by steered molecular dynamics simulations and energy calculations

Bing Zhang · Zhou Cheng Su · Tong Earn Tay · Vincent B. C. Tan

Received: 20 September 2009 / Accepted: 15 November 2009 / Published online: 15 December 2009

Abstract In the current work, CDK5/p25 complexes were pulled apart by applying external forces with steered molecular dynamics (SMD) simulations. The crucial interactions between the kinase and the activation protein were investigated and the SMD simulations showed that several activation-relevant motifs of CDK5 leave p25 in sequence during the pulling and lead to an *apo*-CDK2 like CDK5 structure after separation. Based on systematic examination of hydrogen bond breaking and classical MD/molecular mechanics-generalized Born/surface area) (MM-GBSA) calculations, a CDK5 activation mechanism by p25 is suggested. This is the first step towards the systemic development of CDK inhibitors and the mechanism proposed could lead to a better understanding of the protein–protein recognition characteristics between the kinase and its activator.

Keywords Cyclin-dependent kinase · Molecular dynamics · Protein–protein interaction · Steered molecular dynamics

Introduction

Cyclin dependent kinases (CDKs) constitute a family of serine/threonine kinases. They play a central role in the coordination of eukaryotic cell cycles and their activity is usually regulated by binding with cyclins [1–7]. CDK5, however, is a unique member of this family. CDK5 is not involved in cell cycle regulation but plays an indispensable role in the central nervous system (CNS). The kinase was discovered in the early 1990s [8], and great progress has been made since then in characterizing this multifunctional protein. The best known role for CDK5 is in regulating the cytoarchitecture of the CNS [9], but there is also evidence linking CDK5 activity to the regulation of the cytoskeleton, axon guidance, membrane transport, synaptic function, dopamine signaling and drug addiction [8, 10, 11]. Recent investigations have revealed that CDK5 is involved in biological pathways important for several diseases, such as Alzheimer's disease, amyotropic lateral sclerosis (ALS), Parkinson's disease etc. [12–16].

The human p25 and CDK5 proteins were recently coexpressed and crystallized [10, 17]. X-ray diffraction studies have shown that the subunit of the kinase shares a very similar three-dimensional (3D) structure with CDK2 [18]—a very well investigated family member—as reflected in their 60% sequence identity. Both kinases are folded into a typical bi-lobal conformation, comprising an N-terminal domain composed largely of a β-sheet with one helix, the C helix (PSAALRE; PSTAIRE in CDK2)—whose correct orientation is important for catalysis, and a larger C-terminal domain composed of mostly α-helices. A deep ATP-binding cleft (the catalytic site) resides between the two domains. The crystal structure also displays a similar topology for p25 complex with CDK5. Although the activator protein of CDK5, p25, does not share detectable sequence similarity with the cyclins [10] and binds CDK5 with exquisite selectivity, it does not bind appreciably to or activate other members of the CDK family. It presents a cyclin-box fold domain, which is the

B. Zhang · Z. C. Su · T. E. Tay · V. B. C. Tan (✉)
Department of Mechanical Engineering,
National University of Singapore,
9 Engineering Drive 1,
117576 Kent Ridge, Singapore
e-mail: mpetanbc@nus.edu.sg

B. Zhang
Research Centre of Excellence for Mechanobiology,
National University of Singapore,
117609 Kent Ridge, Singapore

structural motif found in the cyclins. The position of this domain relative to CDK5 closely resembles that occupied by cyclin A when bound to CDK2. Interestingly, in spite of all the structural and topological similarities, CDK5 and CDK2 have distinct activation mechanisms [10]. Normally, CDKs are activated by a two-step mechanism, namely, binding of cyclins confers basal kinase activity and phosphorylation of specific amino acids on the activation loop (T-loop) results in full activity [18, 19]. CDK5 is, however, fully activated only by binding of the activating proteins with the T-loop via extensive interactions [10, 20]. The activation loop in free CDK2 cris-crosses the entrance of the catalytic cleft, rendering the ATP inaccessible to the protein substrate [18].

In cyclin A-bound CDK2, the loop stretches away from the entrance of the cleft and stays close to cyclin A. The new conformation substantially relieves the steric hindrances at the entrance to the ATP-binding cleft. The crystal structure of the CDK2/cyclin A complex has contributed to a general model for cyclin binding and CDK activation [18–20].

Because of its high amino acid sequence similarity with CDK2, it is assumed that CDK5 has a similar inactive structure as CDK2 and that the activation mechanism of the kinase by p25 follows that of CDK2 by cyclin A [10, 20]. Despite an abundance of information on CDKs and CDK/activator complexes [21–24], little is known about the dynamic process governed by adhesive interactions during the binding or unbinding of the activators with the kinases. No crystallized *apo*-CDK5 structures are yet available.

Classical molecular dynamics (MD) methods can only be used to simulate systems under equilibrium conditions [25–29]. For those molecules under non-equilibrium conditions, caused, for example, by tensile force, classical MD would need enormously long computational times to achieve the same effect, or the effect would not be observed at all [30]. To be able to simulate processes such as binding or unbinding, the classical method requires the implementation of new algorithms. Steered molecular dynamics (SMD) allows for the application of a time-dependent external force to manipulate biomolecules [30–33]. This can facilitate the unbinding of ligands from proteins and also provides full atomistic details of the process that are not usually available from experimental techniques, such as details of geometry changes [34–39].

In this work, unbinding of p25 from CDK5 is first performed by applying a force with different spring constants. The conformational changes in CDK5 during unbinding are explored by investigating interactions between crucial activation components involved in both CDK5 and p25. By comparing with the results from molecular mechanics-generalized Born/surface area (MM-GBSA) energy decomposition, an unbinding sequence of different parts of the kinase from the activator can be suggested. Finally, a CDK5 activation mechanism is deduced based on all the available unbinding information.

Methods

MD and SMD simulations

Both conventional and SMD simulations were carried out using the AMBER9 program package [40] with the all-atom force field of Cornell et al. [41] on an HP Xeon Two Sockets Quad-Core 64-bit Linux cluster. The starting geometries for the simulations of the complexes were generated from X-ray structure obtained from the Protein Data Bank (PDB ID code: 1UNL). All simulations are at neutral pH. Lys and Arg residues are positively charged and Asp and Glu residues are negatively charged. The default His protonation state in Amber9 was adopted. Counter ions were added to maintain the electroneutrality of all the systems. The classical and SMD systems are immersed in 10 Å and 30 Å layers, respectively, of truncated octahedron periodic boxes of TIP3P water molecules [42]. A 2 fs time step was used in all the simulations and long-range electrostatic interactions were treated with the particle mesh Ewald (PME) [43] procedure using a cubic B-spline interpolation and a 10^{-5} tolerance for the direct-space and with a 12 Å non-bonded cutoff. Bond lengths involving hydrogen atoms were constrained using the SHAKE algorithm [44]. All systems were minimized prior to the production run. The minimization, performed with the SANDER module under constant volume condition, consisted of four steps. All heavy atoms in both proteins and ligands were restrained with *c* forces of 500, 100, 5 kcal mol^{-1}, respectively. In the first three steps, minimization of the solvent molecules and hydrogen atoms of the systems involved 250 cycles of steepest descent followed by 250 cycles of conjugate gradient minimization. All systems were then relaxed by 500 cycles of steepest descent and 1,000 cycles of conjugate gradient minimization in the last step. Then, the systems were heated to 300 K in three steps. The systems were first heated to 100 K during 10 ps and then to 200 K during the next 10 ps, and then to 250 K in another 10 ps. Finally, they were heated to 300 K in the last 20 ps.

The production parts of classical MD took 5 ns in the NPT ensemble at 300 K with Berendsen [45] temperature coupling and constant pressure (1 atm) with isotropic molecule-based scaling [45]. A 150 ps equilibrium run was followed by SMD simulations. Three different spring constants of 1, 10 and 40 kcal $mol^{-1}Å^{-2}$ were applied between CDK5 and p25 to test the effects of different force increments on the protein structures during the unbinding process. The complexes were separated at a speed of 4 m s^{-1}

until the distance between the proteins reached 40 Å, which means the SMD simulation took 1 ns. To keep computational time practicable, the pulling speed was much faster than those used in atomic force microscopy experiments. However, speeds were limited by the computational cost but were still within the reasonable range used in many reported SMD simulations [46–51]. The mass centers of the major atoms that form intermolecular interactions between CDK5 and p25 were specified to be pulled as shown in Fig. 1. The process of the unbinding phenomenon is considered to be dependent on the direction of pulling. However, the direction of pulling itself can be defined in numerous ways, and there is no previous report on the unbinding of CDK5/p25 complex as far as we know. The pulling direction in the current system was assigned on all hydrogen bonding contributor pairs between the kinase and the activator protein for effective separation of the complex.

MM-GBSA calculations

The energy decomposition of the CDK5/p25 complex was analyzed using the MM-GBSA [52] approach to highlight the electrostatic and van der Waal contributions to the binding of the kinase to the activator.

The binding free energies (ΔG_{bind}) are computed as:

$$\Delta\text{Gbind} = \Delta G(\text{complex}) - [\Delta G(\text{protein}) + \Delta G(\text{ligand})] \quad (1)$$

$$\Delta\text{Gbind} = \Delta\text{Egas} + \Delta\text{Gsolv} - \text{T}\Delta\text{S} \quad (2)$$

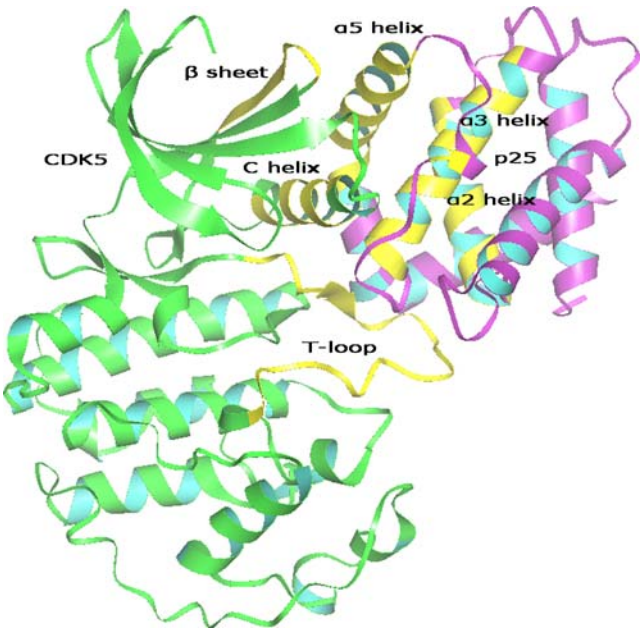

Fig. 1 Pulling sites of CDK5/p25. All pulled motifs are highlighted in *yellow*

$$\Delta\text{Egas} = \Delta\text{Eint} + \Delta\text{Eele} + \Delta\text{Evdw} \quad (3)$$

$$\Delta\text{Gsolv} = \Delta\text{GGB} + \Delta\text{Gnonpolar} \quad (4)$$

The sum of molecular mechanical energies, ΔE_{gas}, can be divided into contributions from internal energy (ΔE_{int}), electrostatic potential (ΔE_{ele}) and van der Waals (VDW; ΔE_{vdw}) potential. The solvation free energy (ΔG_{solv}) is composed of two parts: polar solvation free energy (ΔG_{GB}) and nonpolar salvation free energy ($\Delta G_{\text{nonpolar}}$). All energies are averaged along the MD trajectories. The snapshots are sampled from the last 3 ns single trajectory with an interval of 20 ps. The single trajectory approach is applied to estimate the energies. Estimation of energies in this manner has proven successful in our previous and many other studies [25–28, 53, 54]. Part of the reason for the success of this approach is the cancellation of errors that mask the effect of incomplete sampling. A better approach is the use of separate trajectories of protein–ligand complex, free protein, and free ligand. Unfortunately, due to sampling limitations, the separate trajectory approach appeared to be significantly less stable in numerical study. E_{gas} is obtained using SANDER, and estimation of ΔG_{GB} was conducted with a built-in module, GBSA in AMBER. G_{nonpolar} was determined from Eq. 4,

$$\Delta\text{G}_{\text{nonpolar}} = \gamma\text{A} + \text{b} \quad (5)$$

where A is the solvent-accessible surface area (SASA) estimated using Sanner's algorithm [55] with a solvent probe radius of 1.4 Å and the PARSE atomic radii parameters [56]. γ and b are empirical constants and are set to 0.00542 and 0.92 kcal mol^{-1}, respectively.

Results and discussion

Influences of different spring constants on unbinding

Different spring constants were applied between CDK5 and p25 to explore the influences of different force increments on the conformations of the proteins during the unbinding processes. The rupture force vs time, the root mean square deviation (RMSD) values of the CDK5/p25 complexes, the CDK5 and p25 units, and the C-helix and T-loop parts of CDK5 generated from the three sets of SMD simulations are shown in Fig. 2. According to Bell's model (Eq. 6) of specific adhesion under applied force F_R [33, 57–59], when the pulling speed is fixed, within the same time span, a larger spring constant means a faster time-dependent increase in rupture force during a pulling manipulation, as described in Fig. 3.

$$F_R = \frac{k_B T}{x_b} \ln \frac{F' x_b}{k_B T k_{off}} \quad (6)$$

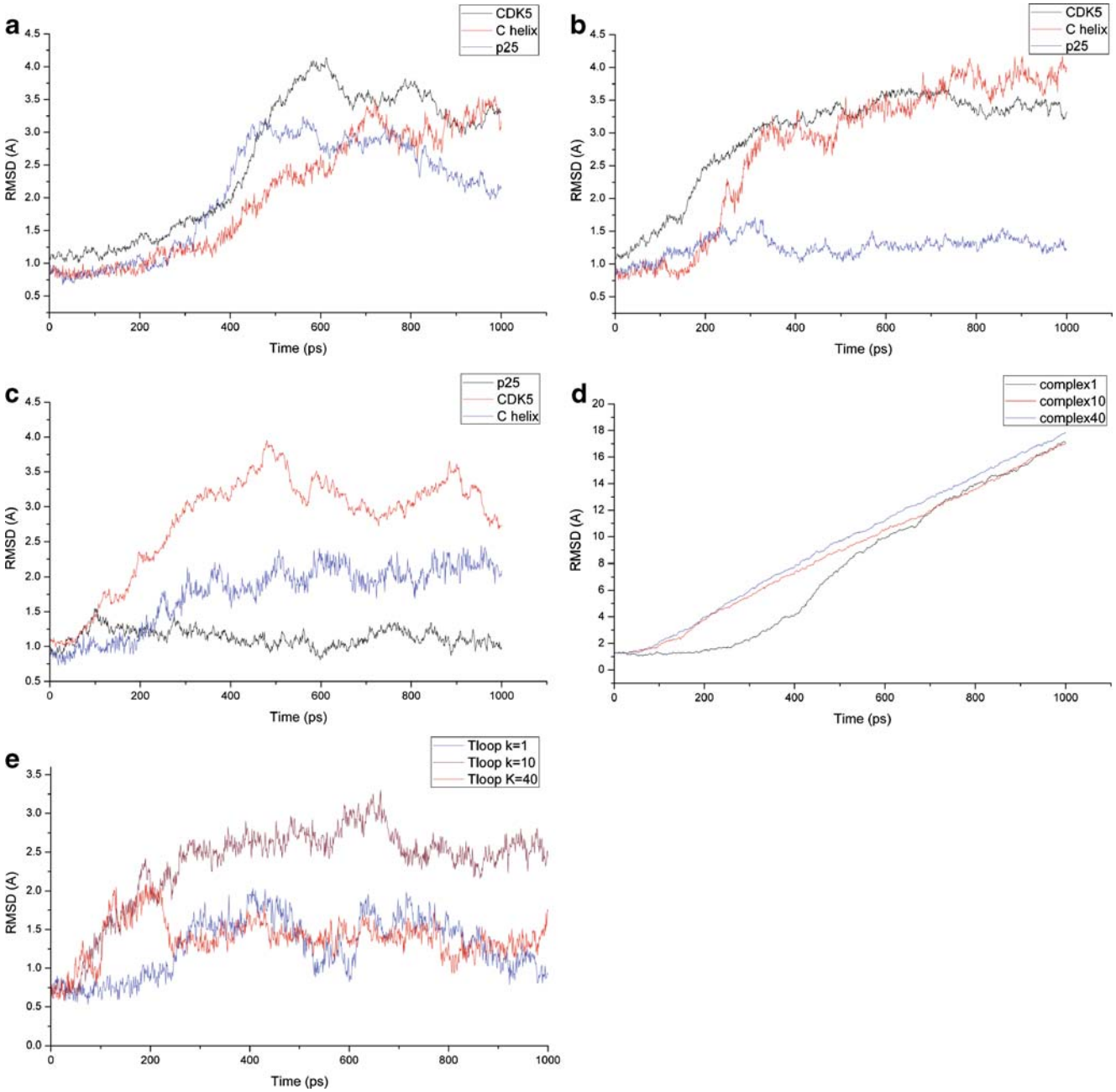

Fig. 2 The root mean square deviation (RMSD) values of CDK5, p25, the C helix when the spring constants (k) are **a** 1 kcal mol^{-1} Å^{-2}, **b** 10 kcal mol^{-1} Å^{-2} , and **c** 40 kcal mol^{-1} Å^{-2} , respectively. **d**, **e** RMSD curves of the CDK5/p25 complex and the T-loop for different spring constants

Here, k_B is Boltzmann's constant, T is absolute temperature, x_b is the distance between the bound state and the energetic maximum, $F'=kv$ is the loading rate (where k is the spring constant and v is the velocity), and k_{off} is the kinetic rate of binding dissociation at equilibrium.

Comparing the curves of the RMSD data of CDK5, p25 and the C-helix, from Fig. 2a–c reveals that the pulling operations with spring constants of 1 and 40 kcal mol^{-1} Å^{-2} introduce relatively big fluctuations of the CDK5 unit, as reflected by the larger oscillations in the RMSD curves. For example, as shown in Fig. 2d and Fig. 3, when the spring constant is 1 kcal mol^{-1} Å^{-2}, both the separation of CDK5 and p25 and the unbinding force increase more slowly than the other two simulations. Snapshots of the SMD simulations at 330 ps (when the spring constant is 10 kcal mol^{-1} Å^{-2}) and 620 ps (1 kcal mol^{-1} Å^{-2}), respectively, are extracted and shown in Fig. 4. The figure shows that when the structures are superimposed, there is very little change in the positions

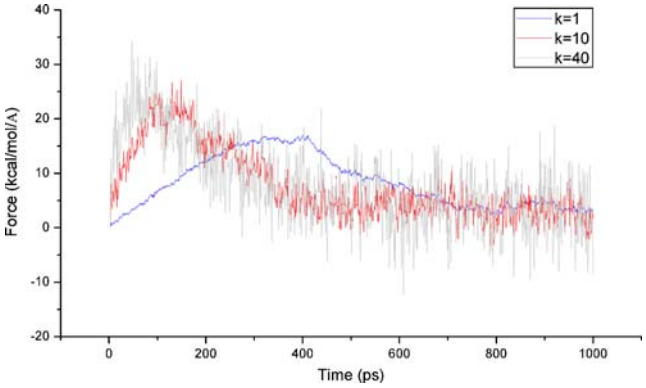

Fig. 3 Force vs time curves for different spring constant (k) settings

of the α5 helix of p25 from one snapshot to the other but obvious differences in the rest of the activator. Furthermore, as can be seen in Fig. 2a,b, the RMSD values of p25 at the 620 ps and 330 ps are around 2.75 Å and 1.25 Å, respectively. This means a much slower displacement of the α5 helix and a bigger distortion of p25 when the spring constant is smaller. The same fluctuation of CDK5 happens when the force constant is increased to 40 kcal $mol^{-1}Å^{-2}$ (Fig. 2c). It seems, from the above observations, that a different force constant introduces a different force increase when the pulling speed is fixed; however, when the unbinding force increases too slowly, the unbinding process needs more time to separate the complex, which probably leads to bigger distortion of the proteins. On the other hand, when the unbinding force increases too fast, the unbinding might happen in less time, but results in bigger distortion. In the present unbinding system, the spring constant 10 kcal $mol^{-1}Å^{-2}$ showed a reasonable value to give a balance between proper force increase and stability of the simulations, and was therefore chosen for subsequent SMD data collection.

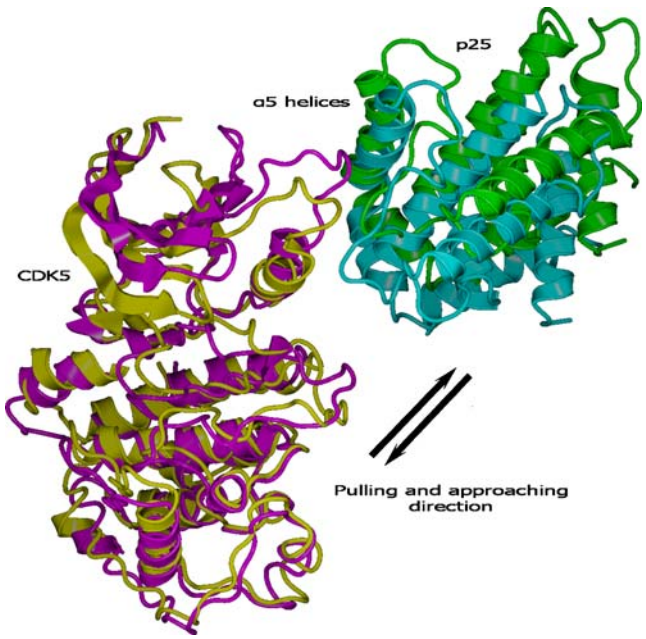

Fig. 4 Superimposed snapshots at 330 ps (CDK5 is in *yellow*; p25, *blue*; *k*=10) and 620 ps (CDK5, *purple*; p25, *green*; *k*=1)

Conformational changes of the C helix and the T-loop

Obvious conformational changes in the C helix and the T-loop were observed during the unbinding processes (Fig. 2b,e). As shown in Fig. 5, the C helix, together with the loop preceding the helix (hereafter, p-loop) apparently displaces from its original location towards the p25 side. The distances between the CA carbon atoms of the tip amino acid of the p-loop (Gly43) and the starting amino acid of the C helix (Ser46) before and after pulling are

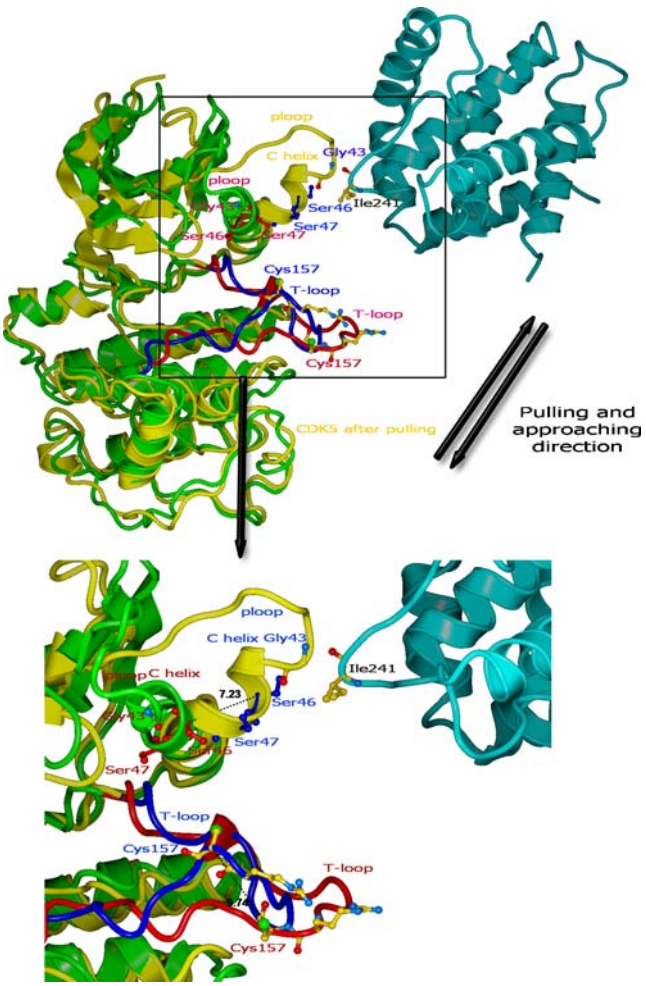

Fig. 5 CDK5 (*yellow*) and p25 (*blue*) after pulling and the original CDK5 (*green*). The distorted and the original T-loops are colored *blue* and *red*, respectively, for clarity. The amino acids Ser46, Ser47 and Cys157 in the stretched and original CDK5 are highlighted in *blue* and *red*, respectively. In this picture, the snapshot of p25 leaving CDK5 at the last moment is adopted to illustrate the departure of the activator

14.15 Å and 7.23 Å, respectively. This displacement of the C helix brings it back to a location very similar to that of the conformation of its counterpart in *apo*-CDK2 (Fig. 6). Instead of the stretched conformation in the initial CDK5/p25 combination, the T-loop adopts a curled appearance, tilting up toward the ATP-binding cleft side, which again resembles the T-loop topology and conformation in *apo*-CDK2 [18]. The distance between the alpha carbon atoms of Cys157 on the T-loop before and after the unbinding is 9.74 Å.

Hydrogen bonding analyses during the unbinding process

Hydrogen bonding (HB) drives strong noncovalent interactions. The analyses of the crystal structures of CDK5/p25 [10] probe extensive electrostatic and VDW interactions between the β sheet and a small loop following the C helix (hereafter, f-loop) of CDK5 and the α5 helix of p25 (the motifs of p25 are named and labeled according to reference [10]). Important HB and distances between the crucial amino acids of CDK5 and p25 during unbinding are traced and listed in Table 1. Several selected distances are also described in Fig. 7. From the figure, it is evident that some of the distances appear very stable at the beginning of the pulling and just start increasing abruptly, and almost linearly, after some time (Fig. 7a,b); the phenomenon involves only the HB distances listed in Table 1. The sudden increase in the distances implies the breaking of HB between the amino acids. The two curves, representing distances of Ser46/Ile241 and Ser47/Ile241 (Fig. 7c), show an interesting trend during unbinding. They reveal that the serines located at the end close to the p-loop of the C helix establish stable HB interactions with Ile241 in tandem during a time span of about 500 ps when the complex is being pulled apart. The total duration time of the two HBs is clearly longer than that of the other HBs. Additionally, the curve in Fig. 7d, which marks the changes in distance between the p-loop of CDK5 and the α3–α4 loop of p25, displays a relatively slow and smooth increase. This is likely due to the fact that flexible loop–loop interactions normally afford bigger conformational distortions. In this case, the p-loop is dragged away slowly from its original position towards the p25 pulling direction.

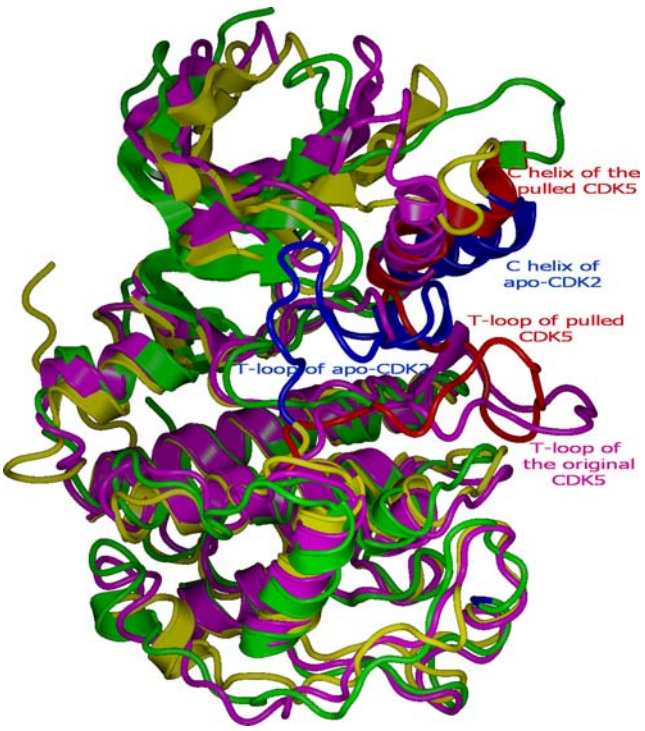

Fig. 6 Superimposition of the original CDK5 (*purple*), the stretched CDK5 (*green*, the T-loop is highlighted in *red*), and the *apo*-CDK2 (T-loop in *blue*)

Energy decomposition of crucial interacting motifs of CDK5

From the crystal structure [10], the C helix, β sheet and T-loop of CDK5 are found to be the central motifs interacting with p25. MM-GBSA energy decomposition was carried out to investigate the binding properties and the unbinding behaviors of the different parts of the kinase. Both the electrostatic and VDW energy contributions from the crucial amino acids of the motifs of CDK5 are listed in Table 2. The total energy contribution, including the effect from solvent water molecules, are also given as references.

From the table, it can be observed that the VDW and electrostatic contributions from the T-loop (21 residues 145–165), −495.47 kcal mol^{-1}, are much weaker than that of the C helix (11 residues 45–55)/β sheet (9 residues 65–73) part, −711.59 kcal mol^{-1}, during the interaction with p25. This means that unbinding of the T-loop area from p25 is easier than from the helix/sheet motifs area. The interaction energy of the T-loop of CDK5 and CDK2 with p25 and cyclin A, respectively, has been implied as being crucial to the binding of both the kinase and activation proteins [20]; our calculations seem to support those conclusions and further indicate that the loop of CDK5 is not the tightest binding motif with p25. Compared with the energy contributions from the 21 residues of the T-loop, interactions offered by the nine amino acids of the β sheet (−318.65 kcal mol^{-1}) are apparently tighter. However, when compared with the energy contributions from the β sheet and the C helix, the data reveal the tightest binding with a value −392.94 kcal mol^{-1} contributed from the latter. If the interaction from the p-loop is also taken into account, the −415.01 kcal mol^{-1} energy contribution of C-helix/p-loop could clearly indicate the last segment departing from p25 during unbinding.

Table 1 Hydrogen bonding (HB) analyses

Amino acid of CDK5	Location	Amino acid of p25	Location
Asp39-OD2	p-loop	Lys254-NZ	α5 helix
Gly43-CA	p-loop	Ile241-CA	α3–α4 loop
Ser46-OG	C h	Ile241-O	α3–α4 loop
Ser47-OG	C helix	Ile241-O	α3–α4 loop
Ser46-OG	C helix	Tyr243-N	α3–α4 loop
Lys56-NZ	C helix	Asn266-OD1	α5 helix
Glu57-OE1	f-loop	Ser270-OG	α5 helix
Glu57-OE2	f-loop	Ser270-OG	α5 helix
Glu57-OE1	f-loop	Ser269-OG	α5 helix
Glu57-OE2	f-loop	Ser269-OG	α5 helix
His71-NE2	β sheet	Glu255-OE1	α5 helix
His71-NE2	β sheet	Glu255-OE2	α5 helix
His71-NE2	β sheet	Asp259-OD1	α5 helix
His71-NE2	β sheet	Asp259-OD2	α5 helix
Cys157-SG	T-loop	Asn239-ND2	α3–α4 loop
Cys157-O	T-loop	Asn239-ND2	α3–α4 loop

A deduced activation mechanism of CDK5 by p25

The HB analyses and the energy decomposition results seem to suggest that the T-loop, the β sheet and the C helix are the crucial domains of CDK5 interacting with p25, and also imply an orderly displacement of the three different motifs from p25. The T-loop, as a weak interacting part, leaves p25 first, almost at the beginning of the pulling. The HB interactions between the Cys157 on the T-loop and the Asn239 on the α3–α4 loop of p25, however, still initiate an obvious conformational change of the loop, resulting in a conformation similar to the T-loop in *apo*-CDK2. With further pulling, rupture of HBs between the rigid β sheet of CDK5 and the α5 helix of p25 occurs. The HBs experience rapid breaking when the pulling extends about 200–300 ps (10–15 Å), which indicates a separation of the sheet from p25. The C helix/p-loop (CDK5) and α3–α4 loop (p25) interactions turn out to be the last group of unbinding elements between the proteins, which introduce a large displacement of the C helix and make the helix adopt a position and conformation very similar to that of its counterpart in *apo*-CDK2 (Fig. 6). Comparing with the whole structure of *apo*-CDK2, it seems that the total unbinding of p25 leads to an inactive CDK2-like CDK5 structure. Based on all the unbinding information, a reversed process of unbinding is hereby proposed as the activation mechanism of CDK5 by p25.

When p25 approaches CDK5 from the direction depicted in Fig. 5, the α3–α4 loop first interacts with the Ser46 located at the starting section of the C helix to make the first anchor between the two proteins. At the same time, the interactions between the α3–α4 loop and the p-loop, for instance, the VDW interactions between the side chain of Ile241 (p25), and the Gly43, push the p-loop preceding the C helix away from its original position to shift towards the ATP-binding pocket side. Along with the continuous displacement of p25, the HB between the Ser46 and the Ile241 is slowly elongated and consequently impaired before it finally breaks. The Ile241 is, however, now close enough to form a stable HB with the next anchor point—Ser47 on the C helix. The HBs in Fig. 7 illustrate clearly that it is during the transition from the breaking and establishment of Ser-Ile HBs (~200–320 ps) that the HB network between the f-loop and the β sheet and the α5 helix of p25 starts to become organized (~100–300 ps). The time overlap of the ~200–320 ps and the ~100–300 ps indicates that the α5 helix, together with the other components of p25, has arrived at the right position to push the C helix into the catalytic cleft. This is further supported by the big drop in the RMSD curve of the helix, which descends around 300 ps in Fig. 2b. Subsequently, in the presence of the driving force from p25 and the relocation of the p-loop, translation and rotation of the C helix toward the catalytic site is achieved.

According to the RMSD curve of the T-loop, the largest and most important distortion of the loop happens very rapidly in a very short time (<200 ps). When checking the HBs between the loop and p25, interactions between Cys157 and Asn239 were detected, which seem to be crucial for the conformational change. The HBs are built later than the Ser47–Ile241 bonding (~100–200 ps, Fig. 7e), and could have been formed during the final phase of the displacement of the C helix into the ATP-binding cleft. The tip of the α3–α4 loop approaches the T-loop to block the entrance of the binding site and construct HBs with Cys157. Following this, the α3–α4 loop pulls the

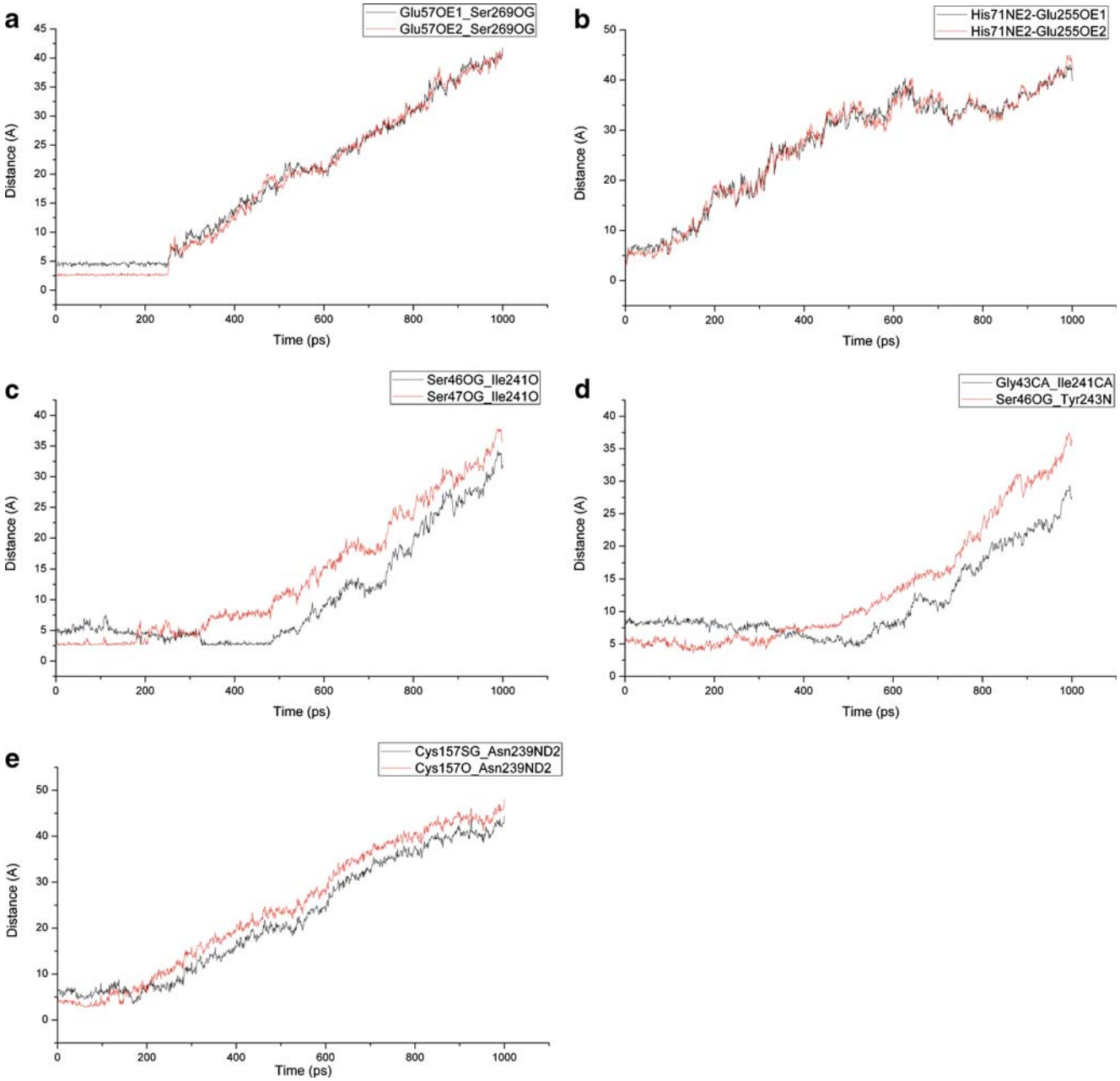

Fig. 7 Analyses of selected hydrogen bonds

T-loop to a stretched conformation with the final motion of p25. The extending loop might facilitate Ile153, the crucial amino acid in recognizing a high hydrophobic site in p25 to fit into its binding pocket. The intensive hydrophobic interactions, as a result, complete the orientation of the T-loop and the whole activation of CDK5. The conformation of the T-loop in the *apo*-like CDK5 does not appear exactly the same as that in the *apo*-CDK2 (Fig. 6), probably

Table 2 Energy decomposition results. *VDW* Van der Waals, *ELE* electrostatic, T_{GB} total energy of the MM/GBSA energy contribution from the amino acids of each motif. Values are in kcal mol^{-1}

	T-loop	C helix	β sheet	C helix+p-loop	C helix+β sheet
VDW+ELE	−495.47	−392.94	−318.65	−415.01	−711.59
T_{GB}	−227.7	−177.78	−161.88	−444.46	−339.66

because, after the leaving of p25, there is no continuous force to drag the loop up and also because the steric interactions from the rest part of CDK5 hamper further distortions.

Conclusions

Protein–protein recognition is deemed the cornerstone of multiple cellular and pathological functions [60, 61]. However, the interaction systems are considered difficult targets, due mainly to the relatively large, featureless interaction surfaces between proteins and lack of starting structures as references. Specific inhibition of a protein kinase is still extremely desirable and remains a challenging goal in inhibitor developments, particularly because of the highly conservative ATP-binding site among the CDK family members [62–64]. New methods or mechanisms to explore new types of inhibitors with good selectivity for CDKs are therefore required. The current work helps to locate the important interaction motifs of CDK5 interacting with p25. The non-equilibrium dynamics simulations and the activation mechanism described here is the first of a multistep development towards selective CDKs inhibitors.

References

1. Harper JW, Adams PD (2001) Chem Rev 101:2511–2526
2. Hunter T, Pines J (1994) Cell 79:573–582
3. Norbury C, Nurse P (1992) Annu Rev Biochem 61:441–470
4. De Azevedo WF, Mueller-Dieckmann HJ, Schulze-Gahmen U, Worland PJ, Sausville E, Kim SH (1996) Proc Natl Acad Sci USA 93:2735–2740
5. De Azevedo WF, Leclerc S, Meijer L, Havlicek L, Strnad M, Kim SH (1997) Eur J Biochem 243:518–526
6. Garrett MD, Fattaey A (1999) Curr Opin Genet Dev 9:104–111
7. Webster KR (1998) Expert Opin Invest Drugs 7:865–887
8. Dhavan R, Tsai LH (2001) Nat Rev Mol Cell Biol 2:749–759
9. Smith DS, Greer PL, Tsai LH (2001) Cell Growth Differ 12:277–283
10. Tarricone C, Dhavan R, Peng J, Areces LB, Tsai LH (2001) Mol Cell 8:657–669
11. Bibb JA, Snyder GL, Nishi A, Yan Z, Meijer L, Fienberg AA, Tsai LH, Kwon YT, Girault JA, Czernik AJ (1999) Nature 402:669–671
12. Nguyen MD, Julien JP (2003) Neurosignals 12:215–220
13. Lau LF, Ahlijanian MK (2003) Neurosignals 12:209–214
14. Smith PD, Crocker SJ, Jackson-Lewis V, Jordan-Sciutto KL, Hayley S (2003) Proc Natl Acad Sci USA 100:13650–13655
15. Bu B, Li J, Davies P, Vincent IJ (2002) J Neurosci 22:6515–6125
16. Wang J, Liu S, Fu Y, Wang JH, Lu Y (2003) Nat Neurosci 6:1039–1047
17. Mapelli M, Massimiliano L, Crovace C, Seeliger MA, Tsai LH, Meijer L, Musacchio A (2005) J Med Chem 48:671–679
18. Jeffrey PD, Russo AA, Polyak K, Gibbs E, Hurwitz J, Massague J, Pavletich NP (1995) Nature 376:313–320
19. Russo AA, Jeffrey PD, Pavletich NP (1996) Nat Struct Biol 3:696–700
20. Otyepka M, Bártovaá I, Kříž Z, Koča J (2006) J Biol Chem 281:7271–7281
21. Anderson M, Andrews DM, Barker AJ, Brassington CA, Breed J, Byth KF, Culshaw JD, Finlay MR, Fisher E, Mcmiken HH, Green CP, Heaton DW, Nash IA, Newcombe NJ, Oakes SE, Pauptit RA, Roberts A, Stanway JJ, Thomas AP, Tucker JA, Walker M, Weir HM (2008) Bioorg Med Chem Lett 18:5487–5492
22. Huwe A, Mazitschek R, Giannis A (2003) Angew Chem Int Ed 42:2122–2138
23. Bettayeb K, Oumata N, Echalier A, Ferandin Y, Endicott JA, Galons H, Meijer L (2008) Oncogene 27:5797–5807
24. Oumata N, Bettayeb K, Ferandin Y, Demange L, Lopez-Giral A, Goddard ML, Myrianthopoulos V, Mikros E, Flajolet M, Greengard P, Meijer L, Galons H (2008) J Med Chem 51:5229–5242
25. Zhang B, Tan VBC, Lim KM, Tay TE (2006) J Comput Aided Mol Res 20:395–404
26. Zhang B, Tan VBC, Lim KM, Tay TE (2007) Biochemistry 46:10841–10851
27. Zhang B, Tan VBC, Lim KM, Tay TE, Zhuang SL (2007) J Mol Model 13:79–89
28. Zhang B, Tan VBC, Lim KM, Tay TE (2007) J Chem Info Model 47:1877–1885
29. Zhuang SL, Zou JW, Jiang YJ, Mao X, Zhang B, Liu HC, Yu QS (2005) J Med Chem 48:7208–7214
30. Orzechowski M, Cieplak P (2005) J Phys: Condens Matter 17: S1627–S1640
31. Sotomayor M, Schulten K (2007) Science 316:1144–1148
32. Hanasaki I, Haga T, Kawano S (2008) J Phys: Condens Matter 20:255238–255347
33. Walton EB, Lee S, Van Vliet KJ (2008) Biophys J 94:2621–2630
34. Zuo ZL, Chen G, Zou HJ, Mok PC, Zhu WL, Chen KX, Jiang HL (2007) Comput Bio Chem 31:186–195
35. Grubmüller H, Heymann B, Tavan P (1996) Science 271:997–999
36. Isralewitz B, Izrailev S, Schulten K (1997) Biophys J 73:2972–2979
37. Izrailev S, Stepaniants S, Balsera M, Oono Y, Schulten K (1997) Biophys J 72:1568–1581
38. Lu H, Isralewitz B, Krammer A, Vogel V, Schulten K (1998) Biophys J 75:662–671
39. Wriggers W, Schulten K (1999) Proteins-Struct Funct Gene 35:262–273
40. Case DA, Pearlman DA, Caldwell JW, Cheatham TE III, Wang J, Ross WS, Simmerling CL, Darden TA, Merz KM, Stanton RV, Cheng AL, Vincent JJ, Crowley M, Tsui V, Gohlke H, Radme RJ, Duan Y, Pitera J, Massova I, Seibel GL, Singh UC, Weiner PK, Kollman PA (2007) AMBER 9. University of California, San Francisco
41. Cornell WD, Cieplak P, Bayly CI, Gould IR, Merz KM, Ferguson DM Jr, Spellmeyer DC, Fox T, Caldwell JW, Kollman PA (1995) J Am Chem Soc 117:5179–5197
42. Jorgensen WL, Chandrasekhar J, Madura JD, Impey RW, Klein ML (1983) J Chem Phys 79:926–935
43. Darden T, York D, Pedersen L (1993) J Chem Phys 98:10089–10092
44. Ryckaert JP, Ciccotti G, Berendsen HJC (1997) J Comput Phys 23:327–341
45. Massova I, Kollman PA (2000) Perspect Drug Discov 18:113–135
46. Heymann B, Grubmüller H (1999) Chem Phys Lett 303:1–9
47. Heymann B, Grubmüller H (2001) Biophys J 81:1295–1313
48. Lu H, Schulten K (1999) Chem Phys 247:141–153
49. Jensen MØ, Park S, Tajkhorshid E, Schulten K (2002) Proc Natl Acad Sci USA 99:6731–6736
50. Park S, Schulten K (2004) J Chem Phys 120:5946–5961
51. Marrink SJ, Berger O, Tieleman P, Jähnig F (1998) Biophys J 74:931–943
52. Gohlke H, Kiel C, Case DA (2003) J Mol Biol 330:891–913

53. Tsigelny I, Greenberg JP, Cox S, Nichols WL, Taylor SS, Ten Eyck LF (1999) Biopolymers 50:513–524
54. Aimes RT, Hemmer W, Taylor SS (2000) Biochemistry 39:8325–8332
55. Sanner MF, Olson AJ, Spehner JC (1996) Biopolymers 38:305–320
56. Sitkoff D, Sharp KA, Honig B (1994) J Phys Chem 98:1978–1988
57. Bell GI (1978) Science 200:618–627
58. Evans E, Ritchie K (1997) Biophys J 72:1541–1555
59. Evans EA, Calderwood DA (2007) Science 316:1148–1153
60. Fry DC, Vassilev LT (2005) J Mol Med 83:955–963
61. Betzi S, Restouin A, Opi S, Arold ST, Parrot I, Guerlesquin F, Morelli X, Collette Y (2007) Proc Natl Acad Sci USA 104:19256–19261
62. Leclerc S, Garnier M, Hoessel R, Marko D, Bibb JA, Snyder GL, Greengard P, Biernat J, Wu YZ, Mandelkow EM, Eisenbrand G, Meijer L (2001) J Biol Chem 276:251–260
63. Noble MEM, Endicott JA, Johnson LN (2004) Science 303:1800–1805
64. Noble M, Barrett P, Endicott J, Johnson L, McDonnell J, Robertson G, Zawaira A (2005) Biochim Biophys Acta 1754: 58–64